

Contents lists available at ScienceDirect

Chemosphere

journal homepage: www.elsevier.com/locate/chemosphere





Mechanistic understanding of perfluorooctane sulfonate (PFOS) sorption by biochars

Samuel Krebsbach ^a, Jianzhou He ^a, Sushil Adhikari ^b, Yaniv Olshansky ^c, Farshad Feyzbar ^d, Leonard C. Davis ^e, Tae-Sik Oh ^d, Dengjun Wang ^{a,*}

- ^a School of Fisheries, Aquaculture and Aquatic Sciences, Auburn University, Auburn, AL 36849, USA
- ^b Biosystems Engineering Department, Auburn University, Auburn, AL 36849, USA
- ^c Department of Crop, Soil, and Environmental Sciences, Auburn University, Auburn, AL 36849, USA
- ^d Department of Chemical Engineering Auburn University, Auburn, AL, 36849, USA
- ^e Department of Biological and Environmental Sciences, East Central University, Ada, OK, 74820, USA

HIGHLIGHTS

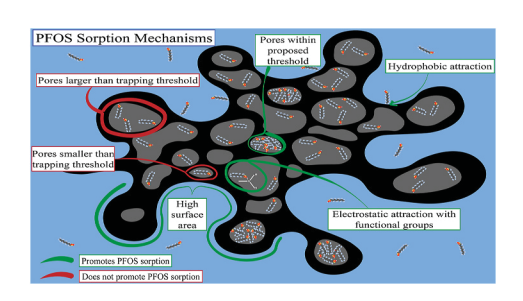
- Biochars pyrolyzed from five feedstocks at three pyrolysis temperatures were used to sorb PFOS from water.
- Biochars pyrolyzed at the highest temperature (900 °C) exhibited the greatest sorption efficiency for PFOS.
- Structural equation model (SEM) analyses identified key physicochemical properties of biochars controlling PFOS sorption.
- Biochars were demonstrated as a costeffective and efficient sorbent for PFOS removal from water.

ARTICLE INFO

Handling Editor: Yongmei Li

Keywords:
Perfluorooctane sulfonate (PFOS)
Biochar
Sorption
Physicochemical properties
Structural equation model

GRAPHICAL ABSTRACT



ABSTRACT

Biochar has recently emerged as a cost-effective solution to combat per- and polyfluoroalkyl substances (PFAS) pollution in water, but mechanistic understanding of which physicochemical properties of biochars dictate PFAS sorptive removal from water remains elusive. Herein, 15 biochars were pyrolyzed from five feedstocks (corn, Douglas fir, eucalyptus, poplar, and switchgrass) at three pyrolysis temperatures (500, 700, and 900 °C) to investigate their removal efficiencies and mechanisms of perfluorooctane sulfonate (PFOS) from water. A commercial biochar was also included for comparison. Biochar physiochemical properties, including elemental composition, pH, specific surface area (SSA), pore structure, hydrophobicity, surface charge, surface functional groups, and crystalline structure were systematically characterized. Batch sorption data showed that the Douglas fir 900 biochar (Douglas fir and 900 are the feedstock type and pyrolysis temperature, respectively; this naming rule applies to other biochars), poplar 900 biochar, and commercial biochar can remove over 95% of PFOS from water. Structural equation model (SEM) was used to elucidate which biochar properties affect PFOS sorption. Interestingly, biochar pore diameter was identified as the most critical factor controlling PFOS removal, but pore diameter/pore volume ratio, SSA, pyrolysis temperature, hydrophobicity, and elemental composition all played variable roles. Hypothetically, biochars with small pore diameters and large pore volumes had a narrow yet deep pore structure that traps PFOS molecules inside once already sorbed, resulting in an enhanced PFOS sorption. Biochars with small pore diameter, low nitrogen content, and high pyrolysis temperature were also favorable for

E-mail address: dzw0065@auburn.edu (D. Wang).

^{*} Corresponding author.

1. Introduction

Per- and polyfluoroalkyl substances (PFAS) have been extensively used in various products such as aqueous film-forming foams (AFFFs), surfactants, paints, and adhesives since the early 1940s (Glüge et al., 2020; Zhang et al., 2021). PFAS have recently garnered global concerns as contaminants, that pose severe hazards to the surface water, groundwater, and drinking water (Lyu et al., 2022). PFAS, such as perfluorooctanoic acid (PFOA) and perfluorooctane sulfonate (PFOS), are recalcitrant against environmental degradation, and consequently have been widely detected in the blood of living organisms and humans (Olsen et al., 2017). In 2016, the U.S. Environmental Protection Agency (EPA) issued a lifetime health advisory level (HAL) for PFOA and PFOS at 70 ng/L combined in drinking water (USEPA, 2016). In June 2022, the U.S. EPA released significantly more stringent HALs for PFOA and PFOS at 0.004 ng/L and 0.02 ng/L, respectively, while adding two new PFAS compounds, perfluorobutane sulfonate (PFBS) and hexafluoropropylene oxide dimer acid (GenX), at HALs of 2000 ng/L and 10 ng/L respectively (USEPA, 2022). This swift, increasingly stringent legislation change galvanizes the direst need to remove PFAS from water.

There are several approaches to effectively remove PFAS from water, such as reverse osmosis, nanofiltration, and sorption using activated carbon (AC), including granular activated carbon (GAC) and powered activated carbon (PAC). AC is a carbonaceous material pyrolyzed from substances with high carbon and low inorganic contents (Ioannidou and Zabaniotou, 2007; Thompson et al., 2016). For water treatment purposes, the particle size of AC needs to be decreased to increase specific surface area (SSA) for a better sorptive performance. After size decrease, the AC is referred to as GAC or in some cases finer PAC (Najm et al., 1991; Newcombe et al., 1993). Both GAC and PAC have been successfully used to remove PFAS in wastewater treatment plants (WWTPs) (Suffet, 1980; Heijman and Hopman, 1999; Oh et al., 2006; Sagbo et al., 2008; Xing et al., 2008; Appleman et al., 2014; Choe et al., 2022). Generally, SSA and hydrophobicity are reported as two main properties for the efficient removal of PFAS by AC. GAC is efficient at removing long-chain PFAS, but certain detrimental weaknesses especially including high production and operational costs in WWTPs make it undesirable for large-scale applications (Thompson et al., 2016; Alhashimi and Aktas, 2017).

Seeking a more cost-effective, efficient, and sustainable treatment sorbent for PFAS removal is critical, as the treatment costs of PFAS remediation ultimately fall to the taxpayers (Cordner et al., 2021). Some of the highest PFAS concentrations were reported near industrial and WWTP discharge sites, as well as fire-training areas at military bases and airports (EWG, 2022). For instance, alarming PFAS concentrations were reported at 6-51 mg/L in soil porewater and groundwater near a military base with a historical use of AFFFs (Adamson et al., 2022), which were 9-10 orders of magnitudes higher than the new EPA HALs (e.g., 0.004 ng/L for PFOA) (USEPA, 2022). Since PFAS cannot be easily removed by conventional treatment techniques, their concentrations are expected to be elevated in areas surrounding municipal and industrial outflows (Appleman et al., 2014; Sörengård et al., 2020; Liu et al., 2021). These areas with high PFAS concentrations require urgent remediation actions to ensure safe water to the public. Hence, an efficient and cost-effective remediation technique is needed to combat the widespread PFAS pollution.

Similar to AC, biochar is a low-density carbonaceous material, produced by the pyrolysis of agricultural and forestry wastes in an oxygen-limited environment (Beesley and Marmiroli, 2011; Yuan et al., 2011; Regmi et al., 2012; Li et al., 2020). Biochar is seen as the precursor of AC

since both can be derived from similar materials (AC can also be produced from coal), but biochar is produced at lower pyrolysis temperatures. This signifies that biochar has richer surface functional groups than AC, due to the lower pyrolysis temperatures (Valdés et al., 2002; Han et al., 2013). The lower pyrolysis temperature coupled with the waste derived feedstocks inherently makes biochar more cost-effective, tunable, and energy-efficient compared to AC. For example, the energy demand, average greenhouse gas emission, and price tag between biochar and AC are reported at 6.1 vs. 97 MJ/kg, 0.9 vs. 6.6 kg CO₂ eq/kg, and \$350-1200 vs. \$1100-1,700, respectively (Thompson et al., 2016; Alhashimi and Aktas, 2017). Furthermore, biochar has also shown to offer carbon sequestration and energy production benefits during pyrolysis, compared to AC (Thompson et al., 2016). Additionally, biochar sorptive removal of PFAS is expected to be promising, due to high SSA, rich functional groups, hydrophobicity, and tunable surface functionalities (Chen et al., 2011). All these benefits clearly suggest biochar holds a high promise to remove PFAS from water.

While promising, the current knowledge on which biochar types, what physicochemical properties of biochars, and the extent to which biochars can remove PFAS from water remain largely unclear. Therefore, the main objective of this research was to provide an in-depth investigation into biochar physiochemical properties for PFAS removal from water. PFOS was selected as a model PFAS compound to mechanistically explore their sorption mechanisms by biochars, since PFOS is always a top priority PFAS representative under stringent regulations in drinking water by federal and state agencies (e.g., U.S. EPA) (USEPA, 2016, 2022; 2023). Physicochemical properties of biochars were systematically characterized, which were then correlated with PFOS sorption data to understand which biochar properties likely control PFOS sorption by statistical analyses. Our new findings shed light on the mechanistic understanding for the development of next-generation biochars for effective and efficient removal of PFAS from water.

2. Materials and methods

2.1. Chemicals and reagents

Perfluorooctane sulfonate (PFOS potassium salt) at a purity >95% was purchased from Matrix Laboratories (Mount Prospect, IL). The physiochemical properties of PFOS were shown in the Supplementary Information (SI) Table S1. Sodium chloride (NaCl) was purchased from Acros Organics (Fisher Scientific Biotechline A/S, Denmark). ACS-grade methanol was purchased from VWR (VWR Chemicals BDH). Milli-Q water was produced using the Milli-Q Advantage A10 water purification system (Milli-Q, Millipore Sigma, Germany).

2.2. Feedstocks for biochar production

Five feedstocks including corn cob (Zea mays), Douglas fir (*Pseudotsuga menziesii*), eucalyptus (*Eucalyptus* spp.), poplar (*Populus balsamifera*), and switchgrass (*Panicum virgatum*) were used to produce biochars (one commercial biochar was also included for comparison). These five feedstocks include two grasses (corn cob and switchgrass), two hardwoods (eucalyptus and poplar), and one softwood (Douglas fir). Strictly speaking, corn is not classified as a grass feedstock. However, corn's properties are more similar to those of grass feedstock compared to wood feedstock, corn was classified into the grass feedstock category in this study. The five feedstocks were air dried for several days first, followed by further grinding and processing to obtain small particles with sizes roughly ranging from 0.5 to 10 mm, prior to biochar production. Detailed descriptions of all feedstocks were shown in the SI

Table S2.

2.3. Biochar production

A slow pyrolysis process of feedstocks was used to produce biochars at three targeted temperatures of 500, 700, and 900 °C using an MTI 1100X furnace (MTI Corporation, Richmond, CA). The heating gradient started at a rate of 8.5 °C/min from 25 °C to 200 °C, where it was held for 30 min, allowing the furnace to purge any moisture and precisely reach the desired temperature. The same rate of 8.5 °C/min was then used to reach the targeted pyrolysis temperatures (500, 700, and 900 °C) and held there for 30 min to ensure even and complete pyrolysis of the feedstocks. The furnace was then cooled down to 200 °C at a rate of $8.5~^{\circ}$ C/min. Afterwards, the biochar was allowed to cool down to $25~^{\circ}$ C on its own. A detailed depiction of biochar production was given in the SI Fig. S1. Biochar samples were stored in beakers covered by foils inside a desiccator. The commercial biochar was donated by Oregon Biochar Solutions (White City, OR) that was produced in an oxygen limited environment at 1000 °C, but detailed production method was unknown due to intellectual property rights. In total, 16 biochars (15 biochars produced from five feedstocks at three pyrolysis temperatures and one commercial biochar) were used for PFOS removal from water (as shown

One of the easiest ways to increase biochar SSA for better PFOS sorption is to decrease particle size. This was done by ball milling in an MTI planetary ball mill (4 \times 500 mL capacity; MTI Corporation, Richmond, CA). All biochar samples were ball milled at 500 rpm for 3 h, in which 10 mL of methanol was added to the milling jar to facilitate particle breakup. After ball milling, biochar was saturated with methanol and transferred to 50 mL polypropylene centrifuge tubes. The biochar samples were then centrifuged at 9500 rpm for 30 min, and the methanol supernatant was discarded. The remaining biochar/methanol slurry left over was dried for at 70 $^{\circ}$ C in an VWR oven for 24 h to ensure all methanol was completely evaporated. This drying process caused coagulation between biochar particles, so the biochars were then ground using a pestle and mortar and stored in a desiccator for later use.

2.4. Detailed characterization of physicochemical properties of the biochars

The physicochemical properties of biochars, including elemental composition, pH, SSA, pore structure, hydrophobicity, surface charge, surface functional groups, and crystallinity were systematically characterized. Briefly, elemental composition of biochars was analyzed on a Vario MICRO Elementar Analyzer (Ronkonkoma, NY) using the ASTM D5373-21 method (ASTM, 2021). This analysis was performed by using 2-5 mg of biochar, and samples were run in duplicate. The pH of biochar suspensions (0.1 g/L) was measured on the A211 Orion Star pH Meter (Thermo Scientific, Waltham, MA) in triplicate. The nitrogen adsorption/desorption isotherms were measured at 77 K using a Micromeritics MicroActive ASAP 2460 to determine biochar SSA and pore structure. The SSA was obtained according to the Brunauer-Emmett-Teller (BET) equation and total pore volume was calculated by N2 adsorbed amount at a relative pressure of 0.99. Both pore size and pore size distribution were calculated from N2 desorption via the Barrett-Joyner-Halenda (BJH) method, assuming that all pore shapes are cylindrical and the absorbed amount is from both physical adsorption onto the pore walls and capillary condensation in the mesopores (Bardestani et al., 2019).

The contact angle of water droplets was used to assess the hydrophobicity of biochars on a ramé-hart Contact Angle Goniometer (Succasunna, NJ) equipped with the DROPimage software (SI Fig. S2). Biochar hydrophobicity was determined using a modified sessile drop method (Navarathna et al., 2020). Briefly, a double-sided tape was adhered to a microscope slide and a small amount (<0.005 g) of each biochar was spread evenly to form a thin homogeneous layer on the double-sided tape. Contact angles on either side of the water droplets

were measured at a contrast above 80% and a tilt of less than 0.2° . A blank measurement of the double-sided tape was found to have a contact angle of $\sim 90^{\circ}$ ($\pm 2^{\circ}$ to account for instrument error), meaning that the tape was neither hydrophobic nor hydrophilic.

Surface charge and particle size of biochar suspension (0.1 g/L in 1 mM NaCl) were measured in the DTS1070 disposable folded capillary cells on a Malvern Pro Blue Zetasizer Particle size analyzer (Malvern Panalytical Ltd., Malvern, U.K.). Surface functional groups of biochars were measured on a Jasco Fourier-transform infrared (FT-IR 6600) spectrometer using the FT-IR DRIFT method. To do so, biochar samples were mixed with KBr at a mass ratio of ~300: 1 (KBr: biochar), and infrared absorbance was measured between wavenumbers 600 and $4000~\text{cm}^{-1}$ at a scanning rate of 4 cm/s. After obtaining the raw FT-IR spectra, the obtained curves were smoothed and zero corrected using the Jasco Spectra Manager Program. Proto manufacturing AXRD (X-ray diffraction) powder diffraction system (Proto Manufacturing, Taylor, MI) was used to analyze the crystallographic structure of biochars. Biochar samples were prepared by spreading the biochar powders uniformly across a small shallow dish. The dish was then adhered to a magnetic holder on the instrument for analysis. Biochar samples were scanned at a rate of 2.2°/min at 30 mA and 40 kV with 2-theta (20) of 10° and dwelling time of 5 s.

2.5. Batch sorption experiments of PFOS by biochars and PFOS concentration analysis

Batch sorption experiments were conducted to determine the removal efficiency (%) of PFOS by the 16 biochars. The experiments were performed in triplicate using 50-mL polypropylene centrifuge tubes in a total volume of 40 mL. All stock solutions of PFOS, biochar, and NaCl were prepared using Milli-Q water and stored in 1 L polypropylene bottles. For the experiment, biochar and NaCl were diluted to 0.1 g/L and 1 mM, respectively. Biochar suspensions were sonicated and shaken vigorously before spiking to break apart any coagulation that may have occurred. PFOS was spiked last at a concentration of 500 $\mu g/L$ and samples were placed on an orbital shaker for 48 h (sorption equilibrium was achieved within 48 h). Samples were then centrifuged at 9500 rpm for 30 min, and 25 mL of supernatant was pipetted out by passing through two sequentially stacked 0.22 µm polypropylene syringe membrane filters (Thermo Scientific) to remove any excess biochar particles. The first 5 mL of supernatant was discarded to eliminate the interferences of PFAS loss, potentially due to the polypropylene membrane filtration. Then, 0.9 mL of supernatant was transferred to a 2 mL polypropylene microcentrifuge tube and spiked with 0.1 mL internal standard in methanol. Final internal standard concentration was $20~\mu g/L$ in a 90% water 10% methanol solution. Samples were then vortexed and 300 μL of the vortexed samples was transferred to a polypropylene autosampler vial. Samples were stored at 4 °C until analysis (analysis was completed within 2 weeks). PFOS concentrations in the samples were analyzed on the Thermo Scientific Vanquish Binary ultrahigh performance liquid chromatography (UPLC), quadrupole-orbitrap tandem mass spectrometer (MS/MS; Exploris 120, Thermo Scienific). The instrument has a delay column between pump and autosampler (HypersilGOLD, 1.9 μm , 175 Å, 3 \times 50 mm) to separate any PFAS in the LC system and solvents from the analytes. An Accucore RP-MS, 2.6 μm , $2.1\,\times\,100$ mm C18 column was used for UPLC separation of PFOS analytes. Mobile phase composition consisted of 2 mM ammonium acetate in HPLC-grade water and HPLC-grade acetonitrile. Sample injection volume was 10 µL. A constant flow of 0.2 mL/min was maintained in the column at 40 °C. The MS scan range was 100–1000 m/z with a resolution of 60,000, standard automatic gain control (AGC) target, 70% radiofrequency (RF) lens, maximum injection time auto, with EASY-IC run-start on. Details of instrument settings and sample analyses were described in the SI Text S1.

2.6. Statistical analyses

Linear regression models (y = ax + b; where x and y are explanatory variable and response variable, respectively; and a and b are modelfitted constants) in R (Team, 2022) were used to unravel potential relationships between feedstock type, pyrolysis temperature, and biochar physiochemical properties with PFOS removal. Gathered information from these linear regression models were then used to build structural equation model (SEM) for determining which biochar physicochemical properties are most important in controlling PFOS sorption (Byrnes, 2022). This SEM package in R has been widely used in ecology and natural resource fields to explain complex causal relationships among various variables (Karels et al., 2008; Tarka, 2018; Chen et al., 2023), which is the scenario in our study involving five feedstock types, three pyrolysis temperatures, and diverse physicochemical properties. Particularly, SEM enables us to generalize the considered properties and efficiencies of all biochars to narrow down which physiochemical properties of biochars may affect PFOS sorption. Like other multivariable analyses, SEM works the best when the variables of interest are normalized, so direct comparisons can be made. This was achieved by log transforming all data, including pyrolysis temperatures and PFOS removal efficiencies (%). To this end, biochar properties and performance can be compared using standard deviation rather than respective units, allowing direct comparison of which properties carry more weights for PFOS sorption. Three different SEMs were created to identify the most significant physiochemical properties of biochars that impact PFOS sorption, while the best model was discussed in depth. The highest explanation percent (%) of PFOS removal, the lowest Akaike Information Criterion (AIC) weight score, and the strongest influence from biochar pore structure were considered when choosing the best model. Details on model construction and selection were given in SI Text S2. All three SEMs exhibited a non-significant p-value (the null hypothesis of the model is the probability a model with a better fit could be produced) at p < 0.05 level.

3. Results and discussion

3.1. Physicochemical properties of biochars

As expected, biochar was mostly comprised of carbon, with a carbon content ranging from 74.1% (switchgrass 700; meaning biochar was

produced by switchgrass feedstock at 700 °C) to 95.6% (Douglas fir 900) (Table 1 and SI Fig. S3a). Higher contents of nitrogen were observed in biochars produced from grass feedstocks compared to soft and hardwood feedstocks (p < 0.05) (Table 1 and Fig. S3b). The increased nitrogen content was likely due to the naturally higher nitrogen content of grass feedstocks, compared to woody feedstocks. For example, Bransby et al. (1998) found that switchgrass had a higher nitrogen content of 1.26%, while the woody feedstock of poplar had a lower nitrogen content of 0.65% (Özcan et al. (2020). Except for the hardwood feedstocks, the hydrogen content exhibited an inverse relationship with pyrolysis temperature (Table 1 and Table S4). The linear regression model analyses showed that there was no consistently statistical trend between pyrolysis temperature and feedstock type with contents of other elements (e.g., S).

Interestingly, all biochar suspensions were measured neutral or slightly acidic, except for the commercial biochar with unknown production method. Ball milling of biochar was hypothesized to enhance $\rm CO_2$ exposure, making the biochars more acidic. However, this hypothesis was ruled out since there was no significant difference of pH ($\Delta \rm pH=0.01; n=3)$ for the Douglas fir 700 biochars before and after ball milling (6.50 vs. 6.51). Similar pH results were reported for other biochars produced from Douglas fir feedstocks (Wang et al., 2020). Similarly, linear regression model results indicated that there was no significant difference of biochar pH with pyrolysis temperature and feedstock type in this study.

SSA and pore structure of biochars are reported as key properties affecting PFAS sorption. A biochar with higher SSA has more sites for PFOS sorption, but other surface features such as pore diameter and pore volume are also important. As shown in Table 1, most biochars produced at 700 °C exhibited the highest SSA, which is inconsistent with the notion that higher pyrolysis (e.g., 900 °C) produces biochars with higher SSA (higher pyrolysis temperature causes more release of volatile matters and creates more pores) (Chen and Chen, 2009; Shaaban et al., 2014; Tomczyk et al., 2020). Methanol was added during the ball milling to facilitate breakdown of large biochar particles into small ones via grinding. We speculate that ball milling (e.g., methanol presence and grinding) did not proportionally increase the SSA of biochar as a function of pyrolysis temperature. Rather, feedstock property (Table S1), pyrolysis temperature (500-900 °C), and ball milling in the presence of methanol co-determined the SSA of biochars (Table 1), partly due to different interactions/affinities of methanol with biochars from different

Table 1
The production yield, pH, SSA, pore volume, pore diameter, pore diameter/pore volume ratio, and carbon (C), hydrogen (H), nitrogen (N), and sulfur (S) contents of the 16 biochars used in this study.

Biochar sample	PT (°C) ^a	PY (%) b	pН	SSA $(m^2/g)^c$	PV (cm ³ /g) ^d	PD (nm) ^e	PD/PV (nm/cm ³ /g) ^f	C (%)	H (%)	N (%)	S (%)
Corn 500	500	40.8 ± 7.3	6.82 ± 0.03	56.7	0.117	9.18	78.8	83.2	3.02	1.00	0.04
Corn 700	700	33.8 ± 8.1	6.78 ± 0.05	112	0.119	4.00	33.7	86.7	1.83	0.81	0.03
Corn 900	900	21.8 ± 4.4	6.85 ± 0.15	33.6	0.070	33.5	476	86.0	1.36	0.72	0.07
Douglas fir 500	500	38.1 ± 5.3	5.91 ± 0.00	163	0.122	2.70	22.2	84.4	2.99	0.07	0.02
Douglas fir 700	700	27.9 ± 9.0	6.00 ± 0.08	453	0.107	12.8	120	91.3	1.98	0.13	0.01
Douglas fir 900	900	24.1 ± 13	6.09 ± 0.11	410	0.124	10.7	86.2	95.6	0.98	0.31	0.06
Eucalyptus 500	500	51.0 ± 13	6.16 ± 0.01	379	0.117	8.35	71.3	86.6	2.94	0.10	0.01
Eucalyptus 700	700	34.0 ± 5.1	6.70 ± 0.07	134	0.090	7.83	86.9	90.7	1.55	0.19	0.02
Eucalyptus 900	900	19.9 ± 9.5	6.61 ± 0.09	429	0.099	12.0	122	84.3	2.63	0.17	0.02
Poplar 500	500	34.8 ± 16	6.47 ± 0.05	292	0.238	2.59	10.9	88.3	3.09	0.09	0.02
Poplar 700	700	27.1 ± 15	6.51 ± 0.06	393	0.129	14.6	114	87.6	1.79	0.14	0.02
Poplar 900	900	20.9 ± 8.8	6.72 ± 0.09	60.9	0.073	8.02	110	83.8	2.68	1.26	0.07
Switchgrass 500	500	41.6 ± 10	7.03 ± 0.07	121	0.087	16.6	191	83.2	2.59	1.07	0.09
Switchgrass 700	700	30.8 ± 8.9	7.02 ± 0.04	232	0.099	18.8	190	74.1	1.53	0.72	0.06
Switchgrass 900	900	22.4 ± 8.8	5.92 ± 0.01	60.9	0.082	22.7	276	77.9	1.25	0.75	0.07
Commercial	1000	n/a	8.60 ± 0.12	471	0.184	8.94	48.5	83.0	1.71	0.27	0.17

^a Pyrolysis temperature.

^b Production yield.

^c BET specific surface area (SSA).

^d BJH pore volume (PV).

^e BJH pore diameter (PD).

f pore diameter/pore volume ratio.

feedstocks and pyrolysis temperatures. Nevertheless, woody feedstocks (e.g., Douglas fir and poplar) generally produced biochars with a much higher SSA, compared to biochars produced from other feedstocks (i.e., corn and switchgrass) rich in cellulose (Table 1).

Biochar hydrophobicity is expected to be affected by several factors such as porosity, particle size, alkalinity, pyrolysis conditions, feedstock type, O/C molar ratio, and surface functional groups (Gray et al., 2014; Das and Sarmah, 2015; Ojeda et al., 2015; Hassan et al., 2020; Wiersma et al., 2020; Adhikari et al., 2022). All biochars studied had a contact angle $>90^\circ$ (Fig. 1), meaning their surfaces were overall hydrophobic. The Douglas fir biochars were significantly more hydrophobic, while the corn biochars were significantly less hydrophobic at the p < 0.05 level. Biochars produced at 700 °C had a significantly lower contact angle than biochars produced at 500 and 900 °C (p < 0.05). Overall, the hydrophobic propensity of biochar surfaces is expected to sorb hydrophobic PFAS molecules (C–C backbone) via hydrophobic interaction (Lyu et al., 2022).

The biochars were found to have a pH of point of zero charge (pH $_{\rm PZC}$) ranging from 2 to 4 (Fig. 2). At environmentally relevant pH conditions (e.g., pH = 5–9), the biochars were negatively charged (e.g., -25.0 to -58.1 mV; Fig. 2), indicative of electrostatic repulsion between negatively charged biochars and anionic PFOS molecules. The Douglas fir, switchgrass, and commercial biochars were less negatively charged compared to corn and poplar-derived biochars (p < 0.05), suggesting a less electrostatic repulsion between these three biochars with PFOS. However, the small differences of zeta potential among the biochars did not exhibit a significant effect on PFOS (e.g., no significant relationship between zeta potential and PFOS removal at p > 0.05). Therefore, zeta potential was not considered in the SEM analysis. Furthermore, feed-stock type and pyrolysis temperature were found to have a negligible impact on the zeta potential of biochars (p > 0.05), again suggesting that zeta potential should be ruled out during the SEM analysis.

The surface functional groups of biochars after pyrolysis were mainly comprised of carbon (C), oxygen (O), and hydrogen (H). Similar to Keiluweit et al. (2010), we observed an increasing degree of condensation with increasing pyrolysis temperatures in our study. Approximately 10 different characteristic peaks were identified for the produced biochars (Fig. 3 and SI Table S3). These 10 characteristic peaks were at 3627 cm⁻¹ (free O–H stretching of phenolic and alcoholic –OH); 3446

cm⁻¹ (water and H-bonded hydroxyl (-OH) groups); 3053 cm⁻¹ (C-H stretching of substituted of aromatic C); 2927 cm⁻¹ (asymmetric C-H stretching of aliphatic CH_x); 1730 cm⁻¹ (C=O stretching of ketones and carboxylic acids); 1584 cm⁻¹ (C=C stretching of aromatic components); 1383 cm $^{-1}$ (O–H and α –CH $_2$ bending); 1257 cm $^{-1}$ (C–O–C groups and aryl ethers); 1212 cm⁻¹ (C-O-C symmetric stretch in ester groups of cellulose and hemicellulose); and 881-683 cm-1 (various types of substituted C-H bending) (Orgchemboulder; Keiluweit et al., 2010; Chia et al., 2012; Janu et al., 2021). More importantly, biochars produced at low pyrolysis temperatures, particularly at 500 °C, retained most of these functional groups (Fig. 3). However, only two characteristic peaks were identified on the surfaces of the commercial biochar at 1584 cm⁻¹ (C=C stretching of aromatic components and C=O stretching of conjugated ketones and chinons) and 1212 cm⁻¹ (C-O stretching of alkyl aryl ether) (Chia et al., 2012; Janu et al., 2021) (Fig. 3). This could be due to the high pyrolysis temperature (1000 °C) for producing the commercial biochar.

The XRD spectra showed that five different peaks were identified for the 16 biochars (SI Fig. S4). The first peak around 9° is representative of oxygen atoms that may intercalate into interlayer space, which is bonded to the graphite planar surface during the pyrolysis process (Zhang et al., 2018). A wide peak near 25° is indicative of tridymite and graphitic platelets (Rong et al., 2019). Peaks on the downslope of the broad tridymite graphitic peak (26–28°) represent the (0, 0, 2) plane of biochar's graphitic structure and the last broad peak at 45° signifies short-ranged order in graphene oxide layers (Hsiao et al., 2010; Zhang et al., 2018). Overall, the intensity of the broad peak around 45° (graphitic platelets and short ranged order in graphene oxide layers) increased as the pyrolysis temperature was increased (SI Fig. S4). This suggests that the carbonaceous structure in biochars became more ordered at higher pyrolysis temperatures.

Overall, different feedstocks and pyrolysis temperatures tended to produce a wide variety of biochars with different physicochemical properties. All biochars were rich in carbon (74.1–95.6%), but nitrogen content in grass-derived biochars was higher than that of biochars derived from woody feedstocks (Table 1). The pH of biochars was neutral or slightly acidic, while the commercial biochar was alkaline (Table 1). SSA is a function of pyrolysis temperature, feedstock properties, and ball milling, but woody feedstocks produced biochars with

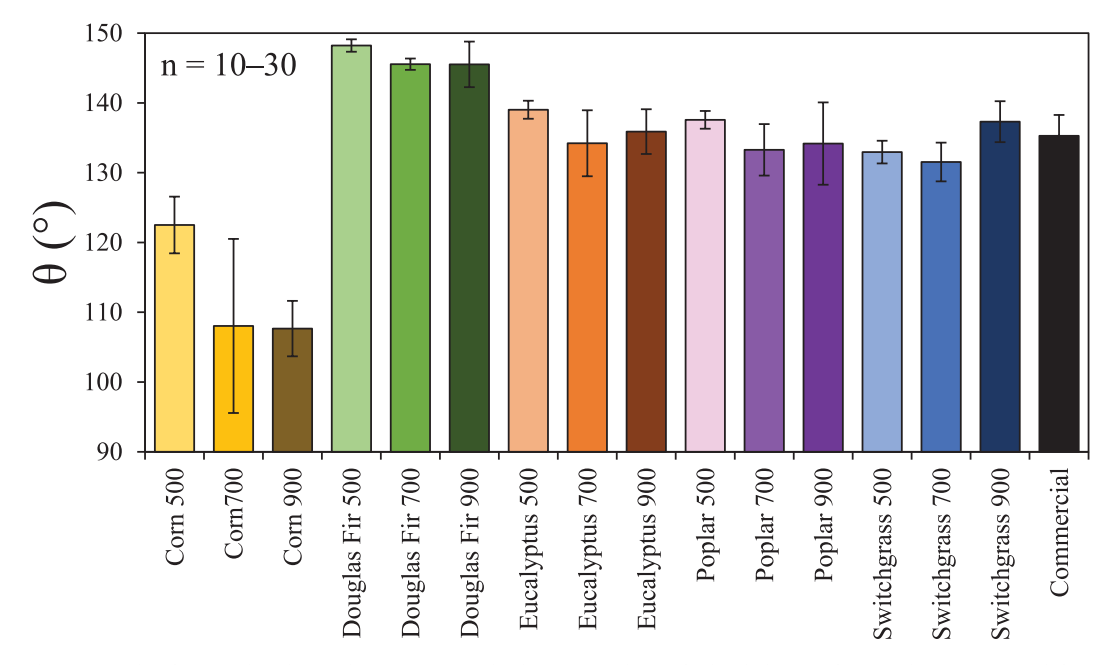


Fig. 1. Contact angle (θ) of 16 biochars used in this study. A contact angle above 90° indicates hydrophobicity. The error bars represented the standard deviations between samples and the number (n) indicates total effective measurements.

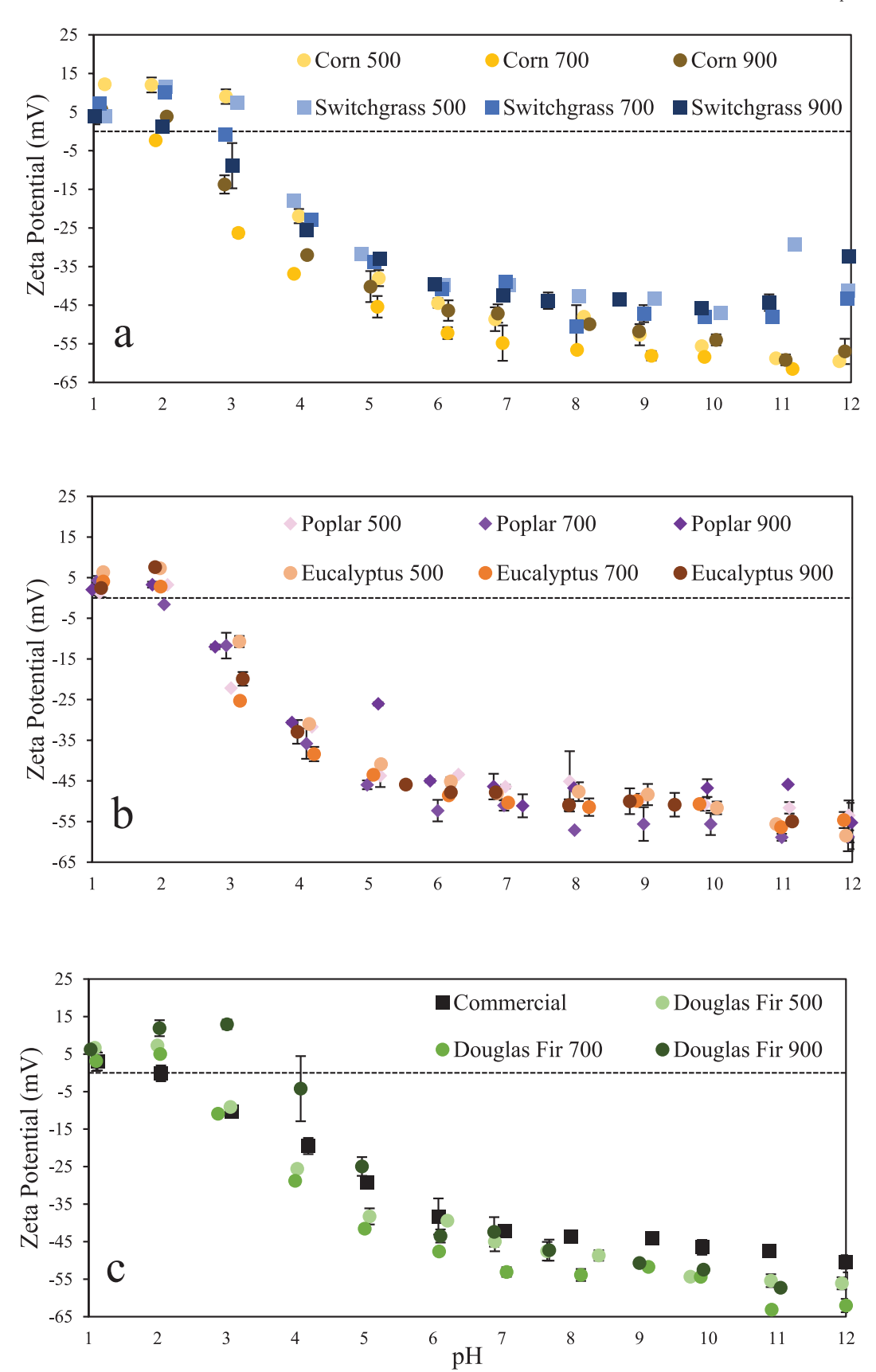


Fig. 2. Zeta potential of (a) grass-, (b) hardwood-, and (c) softwood-derived biochars used in this study. The error bars represented the standard deviations in duplicate experiments.

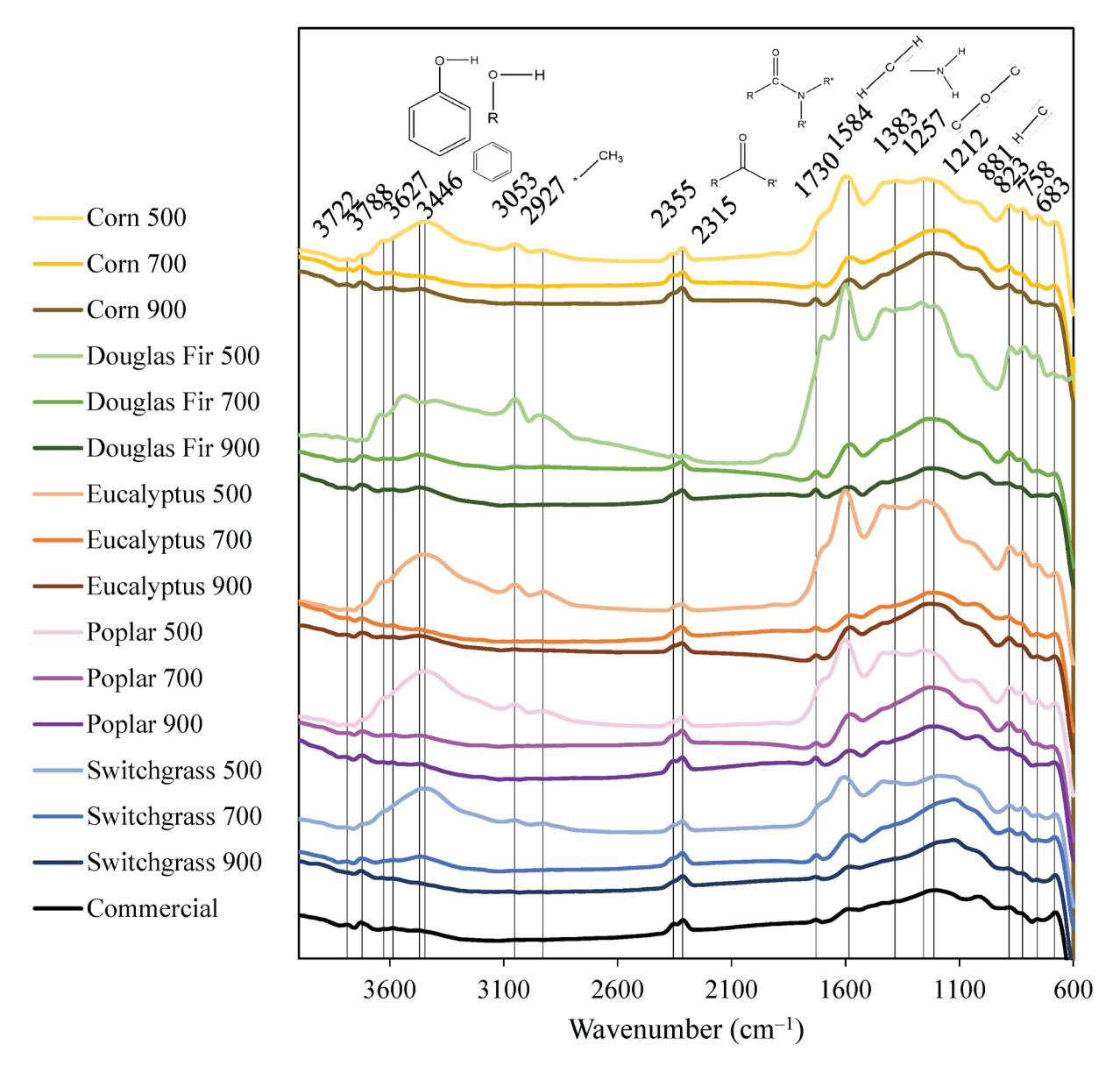


Fig. 3. Fourier-transform infrared (FT-IR) spectra of the 16 biochars. Triplicate experiments were conducted for each biochar sample.

higher SSA than grassy feedstocks. All produced biochars were hydrophobic, with corn feedstocks producing the biochars with the lowest hydrophobicity while Douglas fir biochars having the highest hydrophobicity. Surface charge of biochars ranged from $-25.0\,\mathrm{to}$ $-58.1\,\mathrm{mV}$ at environmentally relevant pH conditions, suggesting electrostatic repulsion between biochars and PFOS. All biochars shared similar characteristic peaks based on FT-IR and XRD spectra, while peak intensities vary mainly as a function of pyrolysis temperatures.

3.2. PFOS sorption by biochars

Batch sorption experiments were used to investigate the removal efficiency (%) of PFOS by the 16 biochars. The Douglas fir 900, poplar 900, and commercial biochars removed >95% of the added 500 μ g/L PFOS from solution (Fig. 4). The observed high removal efficiencies of PFOS were mainly benefitted from the excellent physicochemical properties of biochars (Table 1 and Fig. 1). For example, relatively large specific surface area, suitable pore size, and high hydrophobicity of biochars are expected to be responsible for the high removal efficiency of PFOS by various physical and chemical sorption, as summarized in our recent review study (Lyu et al., 2022). Our linear regression model

analyses showed that pyrolysis temperature was likely a significant factor for PFOS removal. For example, for every 1 °C increase in the pyrolysis temperature, we found a 0.052% ($\pm 0.051\%$; 95% confidence interval (CI)) increase in PFOS removal (p<0.05; $r^2=0.29$). However, biochar produced at one pyrolysis temperature did not significantly outperform another in terms of PFOS removal and there was not one single feedstock type that systematically outperformed other feedstock types with respect to PFOS removal. While biochars derived from woody feedstocks at 900 °C did perform significantly better than other biochars, removing 28.24% ($\pm 13.99\%$; 95% CI) more PFOS than other biochars in this study (p<0.05; $r^2=0.59$) (Fig. 4).

3.3. PFOS sorption mechanisms

Biochar properties vary significantly due to the diversity of their respective feedstocks and pyrolysis temperatures, making trend analysis rather challenging. For example, the corn 900 biochar was found to be an extreme outlier in several physiochemical properties analyzed (e.g., SSA, pore diameter, pore volume, and pore diameter/pore volume ratio) and poplar 500 biochar was also an extreme outlier with respect to pore volume and pore diameter/pore volume ratio. We suspect that the ball

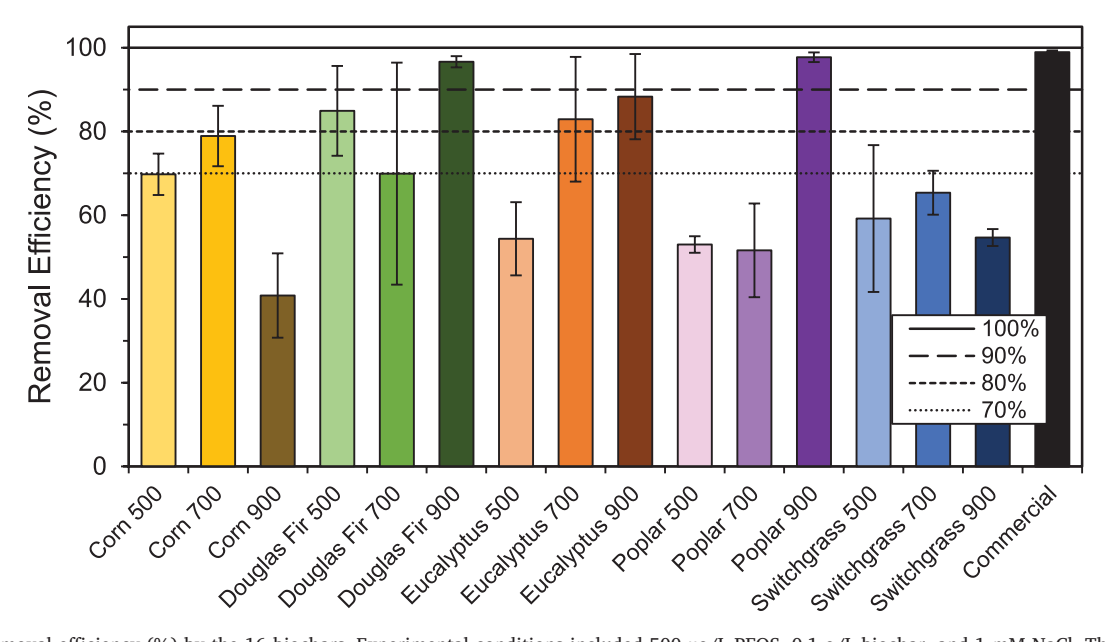


Fig. 4. PFOS removal efficiency (%) by the 16 biochars. Experimental conditions included 500 μ g/L PFOS, 0.1 g/L biochar, and 1 mM NaCl. The error bars represented the standard deviations among triplicate experiments.

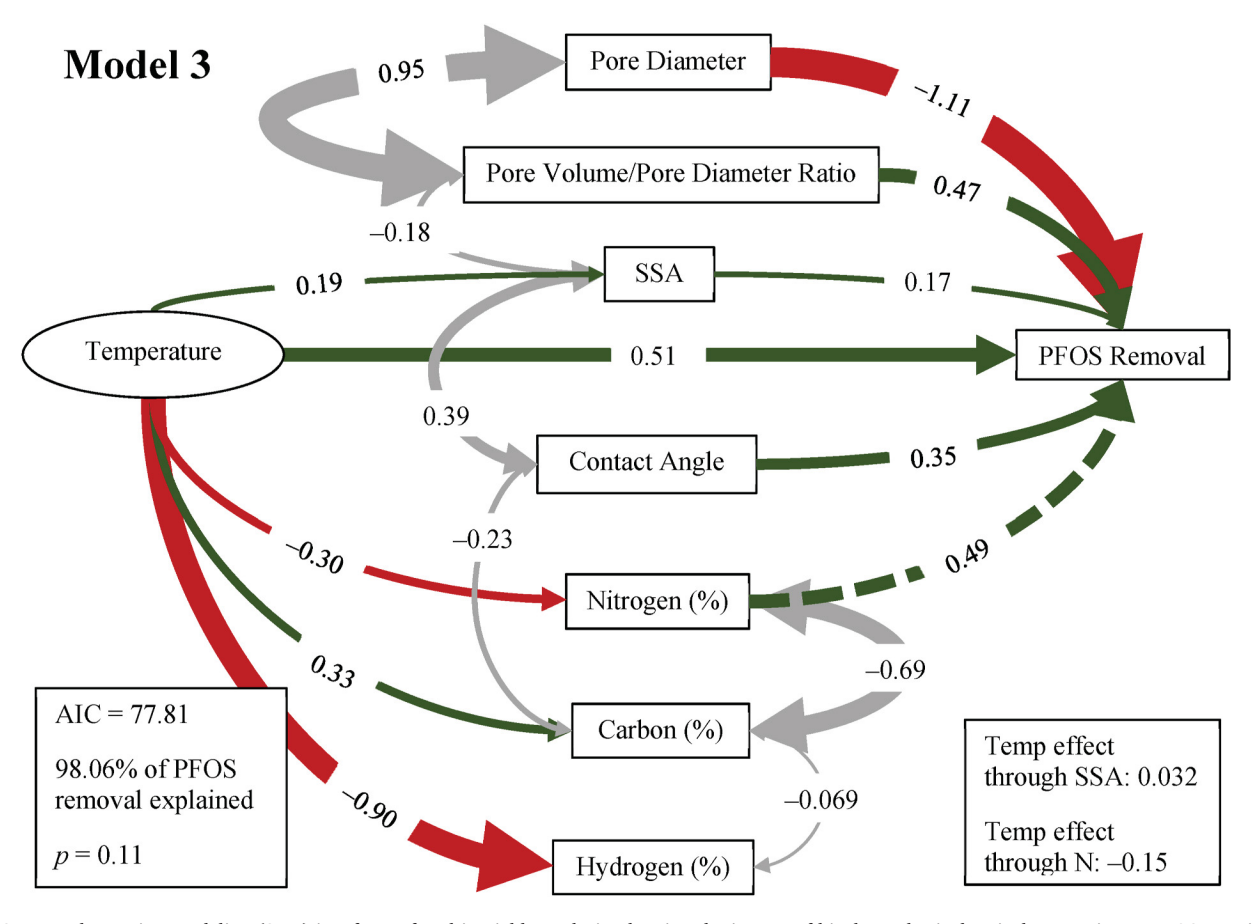


Fig. 5. Structural equation modeling (SEM) is a form of multivariable analysis, showing the impact of biochars physiochemical properties on PFOS sorption. The green arrow indicates a positive relationship between biochar properties and PFOS sorption, while the red arrow indicates a negative relationship. Gray arrows indicate correlations between biochar properties. Numbers on the arrows represent values of each standardized path coefficient, and the arrow width is proportional to the relationship strength (thicker arrow means stronger relationship). The SEM (model 3) has an acceptable goodness of fit score (AIC = 77.81) that can explain 98.06% variation of PFOS removal with a non-significant *p*-value (the null hypothesis of an SEM is a model with good fit) (models 1 and 2 are in SI Fig. S6). The dashed green line between pyrolysis temperature and PFOS removal represents pyrolysis temperatures that indirectly affect PFOS removal. The total effects of pyrolysis temperature through SSA and nitrogen content on PFOS removal can be found in the bottom right corner of the figure. (For interpretation of the references to colour in this figure legend, the reader is referred to the Web version of this article.)

milling procedures to decrease particle size along with feedstock and pyrolysis temperature differences could cause the observed outlier issue for corn 900 and poplar 500 biochars. Adding methanol in the ball milling procedures could also play a role due to potential interaction of methanol with biochars during ball milling. Therefore, both corn 900 and poplar 500 biochars were removed from the dataset before SEM construction. Removing these two biochars allowed for better trend analyses among dependent variables (e.g., when corn 900 and poplar 500 biochars were removed, the r² comparing PFOS removal to pore diameter/pore volume ratio was increased from 0.12 to 0.27).

Feedstock type and pyrolysis temperature are two independent variables in this study, meaning that the selection of a given feedstock at a pyrolysis temperature dictates the outcome of all other dependent variables (e.g., physicochemical properties like SSA, hydrophobicity, and thus PFOS removal efficiency). However, categorical variables would not have worked in this SEM due to the small sample size, so feedstock type was also removed from the model construction. Given that pyrolysis temperature is an independent variable, it does not have a direct impact on PFOS removal. Rather, it affects the individual biochar properties, which in turn affect PFOS sorption. A path coefficient connecting pyrolysis temperature and PFOS removal efficiency enables us to capture the unexplained variables in the model (e.g., zeta potential and pH), which helps explaining the holistic influence of pyrolysis temperature on PFOS removal, as shown in Fig. 5.

While some physiochemical properties of biochars carry more weights for PFOS sorption than others, it is ultimately a combination of properties that differentiate biochars with higher PFOS removal efficiency from the rest. Most notably, pore diameter of biochars was identified as the most important factor for PFOS removal. Specifically, for every 1 standard deviation decrease in pore diameter, there is a 1.11 standard deviation increase in PFOS removal (Fig. 5), suggesting smaller pore diameters have greater PFOS removal efficiency. Another way to interpret the data further is to look at the pore diameter/pore volume ratio (Fig. 5). Specifically, for every 1 standard deviation increase in pore diameter/pore volume ratio, there was a 0.47 standard deviation increase in PFOS removal. These findings clearly suggest the importance of biochar pore structure in PFOS sorption. Logically, there should be a size threshold with respect to how small pore openings can be for a biochar to effectively sorb PFAS molecule. Similarly, there also should be a size threshold in how large a pore diameter can be for effective PFOS sorption. PFOS is reported to have a molecular size of ~1.32 nm (Hassan et al., 2022), so biochars with pores smaller than PFOS molecular size cannot effectively trap PFOS inside their pores (e.g., pore volume, pore diameter, and pore diameter/pore volume ratio data in Table 1). We propose that biochar having an ideal pore diameter range of ~7.5-11 nm (e.g., Douglas fir 900, poplar 900, and commercial biochars in Table 1) can effective sorb PFOS via the 'trapping' mechanism, making it difficult for PFOS to desorb once it is sorbed within the ideal pore structures, but protects the sorbed molecules from water turbulence unlike wider pores (Fig. 6).

This 'trapping' effect for PFOS sorption is expected to be enhanced if the pore volume of biochar is greater, providing more space for PFOS molecules to sorb within the pore structures, i.e., the ideal pore diameter/pore volume ratio being ~50 to 150 (nm/cm³/g). This hypothesis is supported by the data of pore diameters and pore diameter/pore volume ratios shown in Table 1, as well as the PFOS removal efficiency by biochars (Fig. 4). For example, the Douglas fir 900, poplar 900, and commercial biochars all fall within the proposed ideal pore structure range (e.g., pore diameter ≈ 7.5 –11 nm and pore diameter/pore volume ratio $\approx 50-150$ nm/cm³/g; Table 1), that also exhibited the highest removal efficiency for PFOS. The Douglas fir 500 and corn 700 biochars had smaller pores, while all three switchgrass-derived biochars had larger pores (Table 1). The small pores of biochars (Douglas fir 500 and corn 700 biochars) physically preclude the effective entering and thus sorption of PFOS molecules. In contrast, large pores of biochars (three switchgrass biochars) likely provide more opportunities for the trapped

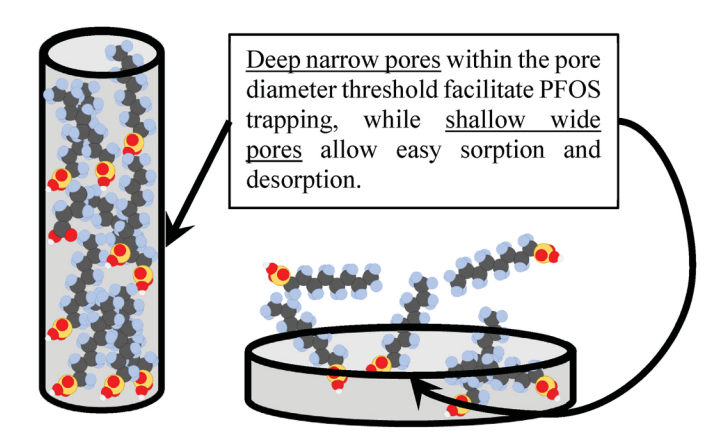


Fig. 6. Schematic illustrating the ability of biochar pore structure to trap PFOS, preventing desorption once already sorbed. Biochars with a pore diameter that is too small to allow enough PFOS to percolate into pores, while biochars with larger pore diameters do not have the ability to trap PFOS.

PFOS molecules to re-entrain back to the aqueous solution due to wider surface areas (Fig. 6). Therefore, these five biochars were observed to exhibit a lower removal efficiency for PFOS, compared to that of Douglas fir 900, poplar 900, and commercial biochars.

While pore structure of biochar was observed to play a crucial role for PFOS sorption, other physicochemical properties of biochars should be scrutinized as well. For example, both corn 500 and eucalyptus 500 biochars fall within the same ideal pore structure range (Table 1), but neither biochars showed high removal efficiency for PFOS, as compared to the Douglas fir 900 or commercial biochars (Fig. 4). However, the Douglas fir 900 and commercial biochars had the highest SSA of all biochars examined, while the corn 500 and eucalyptus 500 biochars showed relatively low SSA (Table 1), partially explaining the observed differences in PFOS removal efficiency (Fig. 6). For example, for every 1 standard deviation increase in biochar's SSA, there was a 0.17 standard deviation increase in PFOS removal (Fig. 5). Overall, the Douglas Fir 900 and commercial biochars fall within the proposed ideal pore structure range and had some of the highest SSA. These findings clearly suggest the importance of both pore structure and SSA for PFOS removal from water. Hydrophobicity also plays an appreciable role in PFOS sorption (Fig. 5). For every 1 standard deviation increase in biochar's contact angle, there was a 0.35 standard deviation increase in PFOS removal, again supporting the notion that PFOS is removed through hydrophobic interactions (Lyu et al., 2022). Given that all biochars were hydrophobic, it is likely that some biochars without the ideal pore structures but having high SSA still have the ability to effective sorb PFOS through hydrophobic interactions (e.g., Douglas fir 500 biochar; Fig. 1). For example, the Douglas fir 500 biochar had a pore diameter of 2.70 nm and a pore diameter/pore volume of 22.2 nm/cm³/g, respectively (Table 1), but still showed a high PFOS removal efficiency of ~85% (Fig. 4). The greatest hydrophobicity of the Douglas fir 500 biochar among all biochars (Fig. 1) may contribute to the high removal efficiency for PFOS in this study.

Elemental composition of biochars varied greatly with pyrolysis temperature (Table 1 and Fig. S3), but S and O contents were not included into the SEM analysis due to their low content (S) and high correlation with other variables (O content), respectively. Interestingly, nitrogen (N) element was found to have the largest impact on PFOS removal (Fig. 5). The positively charged N-containing groups (e.g., amine groups) of biochars are reported to strongly sorb negatively charged PFOS via electrostatic attraction (Fig. 2), accounting for a higher removal efficiency of PFOS by biochars with higher N contents (SI Table S3) (Liu et al., 2022; Lyu et al., 2022). While pyrolysis temperature did not have a direct impact on PFOS sorption, it can directly affect physiochemical properties of biochars for PFOS sorption. In the

SEM analysis, the pyrolysis temperature arrow represents measured factors influencing sorption that were excluded from SEM (e.g., pH, zeta potential, and O content). Again, not all the measured physicochemical properties of biochars were included in the SEM analysis, due to small sample size and singularity errors during model creation (SI Text S2). Similarly, surface functional groups and surface crystallography were precluded from the SEM analysis, since they did not have quantitative results. However, biochars derived from woody feedstocks with less functional groups (Fig. 3) and higher carbon structure ordering (Figs. S4–S5) exhibited higher removal efficiency for PFOS (Fig. 4). PFOS removal by grass-derived biochars was favored at a lower pyrolysis temperature and a higher retention rate of N-containing functional groups (Figs. 3 and 4 and SI Figs. S4–S5).

The SEM analysis with the highest explanation of PFOS removal (98.1%) and relatively low AIC score (77.8) was selected as the best model (Fig. 5). The other two SEM analyses showed 89.0% and 98.0% explanation of PFOS removal with AIC scores of 74.5 and 80.6, respectively (SI Fig. S6). All the three SEMs showed high explanation for PFOS removal and acceptable AIC scores, but model 3 in Fig. 5 was the best since the correlation coefficients explained well how biochar physicochemical properties dictate PFOS removal, as elucidated above.

4. Conclusion

Our findings provide strong evidence to support the feasibility of biochars as a cost-effective and efficient candidate in combatting PFAS pollution from water through sorptive removal. While the trends of biochar physicochemical properties were not consistently changed as a function of pyrolysis temperature, the SEM analyses enabled us to identify which physicochemical properties play an important role for PFOS sorption. Specifically, pore diameter, pore diameter/pore volume ratio, contact angle, and nitrogen content were identified as the most crucial factors controlling PFOS removal. Biochars that have pore diameters between 7.5 and 11 nm, pore diameter/pore volume ratios between 50 and 150 (nm/cm³/g), large SSA, and high hydrophobicity may have high potential to remove PFOS from water. The Douglas fir 900, poplar 900, and commercial biochars can effectively remove over 95% of PFOS at 500 µg/L under 1 mM NaCl. Future research is needed to investigate how biochars perform for PFAS removal under environmentally relevant conditions (i.e., water matrices with organic matter, dissolved ions, and multiple PFAS compounds). Tuning the physicochemical properties of biochars that are important for PFAS sorption could further enhance the performance of biochars for PFAS removal, while saving the treatment cost, especially during large-scale applications (e.g., WWTPs).

Credit author statement

- Sam Krebsbach: Data acquisition and analysis, original draft preparation, and revision.
- Jianzhou He: Writing review and editing.
- Sushil Adhikari: Data acquisition and writing review and editing.
- Yaniv Olshansky: Data acquisition and writing review and editing.
- Farshad Feyzbar: Data acquisition and writing review and editing.
- Leonard Davis: Data acquisition.
- Tae-Sik Oh: Data acquisition and writing review and editing.
- Dengjun Wang: Project administration, conceptualization, methodology, and writing review and editing.

Declaration of competing interest

The authors declare that they have no known competing financial interests or personal relationships that could have appeared to influence the work reported in this paper.

Data availability

Data will be made available on request.

Acknowledgments

This research was supported by the Strategic Environmental Research and Development Program (ER22-3150); U.S. Geological Survey (USGS), Alabama Water Resource Research Institute (G21AS00517); U.S. Department of Agriculture (USDA), National Institute of Food and Agriculture (NIFA), Hatch Program, Alabama Agricultural Experiment Station (ALA016-1-19123); and National Science Foundation-Research Experiences for Undergraduates (REU) for Warm-Water Aquatic Ecology (DBI-1658694). We thank Dr. Dongye Zhao (San Diego State University) and Dr. Ann Ojeda (Auburn University) in guiding the experimental design and data interpretation of this manuscript. Views, opinions, and/or findings contained in this manuscript are those of the authors and should not be construed as an official Department of Defense position or decision unless so designated by other official documentation.

Appendix A. Supplementary data

Supplementary data to this article can be found online at https://doi.org/10.1016/j.chemosphere.2023.138661.

References

- Adamson, D.T., Kulkarni, P.R., Nickerson, A., Higgins, C.P., Field, J., Schwichtenberg, T., Newell, C., Kornuc, J.J., 2022. Characterization of relevant site-specific PFAS fate and transport processes at multiple AFFF sites. Environ. Adv. 7, 100167.
- Adhikari, S., Timms, W., Mahmud, M.A.P., 2022. Optimising water holding capacity and hydrophobicity of biochar for soil amendment – a review. Sci. Total Environ. 851, 158043.
- Alhashimi, H.A., Aktas, C.B., 2017. Life cycle environmental and economic performance of biochar compared with activated carbon: a meta-analysis. Resour. Conserv. Recycl. 118, 13–26.
- Appleman, T.D., Higgins, C.P., Quiñones, O., Vanderford, B.J., Kolstad, C., Zeigler-Holady, J.C., Dickenson, E.R.V., 2014. Treatment of poly- and perfluoroalkyl substances in U.S. full-scale water treatment systems. Water Res. 51, 246–255.
- ASTM, 2021. Standard Test Methods for Instrumental Determination of Carbon, Hydrogen, and Nitrogen in Laboratory Samples of Coal and Coke. ASTM International. ASTM D5373-21).
- Bardestani, R., Patience, G.S., Kaliaguine, S., 2019. Experimental methods in chemical engineering: specific surface area and pore size distribution measurements—BET, BJH, and DFT. Can. J. Chem. Eng. 97, 2781–2791.
- Beesley, L., Marmiroli, M., 2011. The immobilisation and retention of soluble arsenic, cadmium and zinc by biochar. Environ. Pollut. 159, 474–480.
- Bransby, D.I., McLaughlin, S.B., Parrish, D.J., 1998. A review of carbon and nitrogen balances in switchgrass grown for energy. Biomass Bioenergy 14, 379–384.
- Byrnes, J.F.a.Z.N.a.J., 2022. Sem: Structural Equation Models, vol. 3. R package version, pp. 1–15.
- Chen, B., Chen, Z., 2009. Sorption of naphthalene and 1-naphthol by biochars of orange peels with different pyrolytic temperatures. Chemosphere 76, 127–133.
- Chen, F., Niu, Y., An, Z., Wu, L., Zhou, J., Qi, L., Yin, G., Dong, H., Li, X., Gao, D., Liu, M., Zheng, Y., Hou, L., 2023. Effects of periodic drying-wetting on microbial dynamics and activity of nitrite/nitrate-dependent anaerobic methane oxidizers in intertidal wetland sediments. Water Res. 229, 119436.
- Chen, X., Xia, X., Wang, X., Qiao, J., Chen, H., 2011. A comparative study on sorption of perfluorooctane sulfonate (PFOS) by chars, ash and carbon nanotubes. Chemosphere 83, 1313–1319.
- Chia, C.H., Gong, B., Joseph, S.D., Marjo, C.E., Munroe, P., Rich, A.M., 2012. Imaging of mineral-enriched biochar by FTIR, Raman and SEM-EDX. Vib. Spectrosc. 62, 248–257.
- Choe, H.-S., Kim, K.Y., Oh, J.-E., Kim, J.-H., 2022. Parallel study on removal efficiency of pharmaceuticals and PFASs in advanced water treatment processes: ozonation, GAC adsorption, and RO processes. Environ. Eng. Res. 27, 200509-200500.
- Cordner, A., Goldenman, G., Birnbaum, L.S., Brown, P., Miller, M.F., Mueller, R., Patton, S., Salvatore, D.H., Trasande, L., 2021. The true cost of PFAS and the benefits of acting now. Environ. Sci. Technol. 55, 9630–9633.
- Das, O., Sarmah, A.K., 2015. The love-hate relationship of pyrolysis biochar and water: a perspective. Sci. Total Environ. 512–513, 682–685.
- EWG, 2022. PFAS Contamination in the U.S. EWG (June 8, 2022).
- Glüge, J., Scheringer, M., Cousins, I.T., Dewitt, J.C., Goldenman, G., Herzke, D., Lohmann, R., Ng, C.A., Trier, X., Wang, Z., 2020. An overview of the uses of per- and polyfluoroalkyl substances (PFAS). Environ. Sci.: Process. Impacts 22, 2345–2373.

Gray, M., Johnson, M.G., Dragila, M.I., Kleber, M., 2014. Water uptake in biochars: the roles of porosity and hydrophobicity. Biomass Bioenergy 61, 196–205.

- Han, Y., Boateng, A.A., Qi, P.X., Lima, I.M., Chang, J., 2013. Heavy metal and phenol adsorptive properties of biochars from pyrolyzed switchgrass and woody biomass in correlation with surface properties. J. Environ. Manag. 118, 196–204.
- Hassan, M., Du, J., Liu, Y., Naidu, R., Zhang, J., Ahsan, M.A., Qi, F., 2022. Magnetic biochar for removal of perfluorooctane sulphonate (PFOS): interfacial interaction and adsorption mechanism. Environ. Technol. Innovat. 28, 102593.
- Hassan, M., Liu, Y., Naidu, R., Parikh, S.J., Du, J., Qi, F., Willett, I.R., 2020. Influences of feedstock sources and pyrolysis temperature on the properties of biochar and functionality as adsorbents: a meta-analysis. Sci. Total Environ. 744, 140714.
- Heijman, S.G.J., Hopman, R., 1999. Activated carbon filtration in drinking water production: model prediction and new concepts. Colloids Surf. A Physicochem. Eng. Asp. 151, 303–310.
- Hsiao, M.-C., Liao, S.-H., Yen, M.-Y., Liu, P.-I., Pu, N.-W., Wang, C.-A., Ma, C.-C.M., 2010. Preparation of covalently functionalized graphene using residual oxygen-containing functional groups. ACS Appl. Mater. Interfaces 2, 3092–3099.
- Ioannidou, O., Zabaniotou, A., 2007. Agricultural residues as precursors for activated carbon production—a review. Renew. Sustain. Energy Rev. 11, 1966–2005.
- Janu, R., Mrlik, V., Ribitsch, D., Hofman, J., Sedláček, P., Bielská, L., Soja, G., 2021. Biochar surface functional groups as affected by biomass feedstock, biochar composition and pyrolysis temperature. Carbon Resour. Convers. 4, 36–46.
- Karels, T.J., Dobson, F.S., Trevino, H.S., Skibiel, A.L., 2008. Original article: the biogeography of avian extinctions on oceanic islands. J. Biogeogr. 35, 1106–1111.
- Keiluweit, M., Nico, P.S., Johnson, M.G., Kleber, M., 2010. Dynamic molecular structure of plant biomass-derived black carbon (biochar). Environ. Sci. Technol. 44, 1247–1253.
- Li, X., Wang, C., Zhang, J., Liu, J., Liu, B., Chen, G., 2020. Preparation and application of magnetic biochar in water treatment: a critical review. Sci. Total Environ. 711, 134047
- Liu, G., Wei, X., Luo, P., Dai, S., Zhang, W., Zhang, Y., 2022. Novel fluorinated nitrogenrich porous organic polymer for efficient removal of perfluorooctanoic acid from water. Water 14, 1010.
- Liu, N., Wu, C., Lyu, G., Li, M., 2021. Efficient adsorptive removal of short-chain perfluoroalkyl acids using reed straw-derived biochar (RESCA). Sci. Total Environ. 798, 149191.
- Lyu, X., Xiao, F., Shen, C., Chen, J., Park, C.M., Sun, Y., Flury, M., Wang, D., 2022. Perand polyfluoroalkyl substances (PFAS) in subsurface environments: occurrence, fate, transport, and research prospect. Rev. Geophys. 60, e2021RG000765.
- Najm, I.N., Snoeyink, V.L., Lykins Jr., B.W., Adams, J.Q., 1991. Using powdered activated carbon: a critical review. J. AWWA (Am. Water Works Assoc.) 83, 65–76.
- Navarathna, C.M., Bombuwala Dewage, N., Keeton, C., Pennisson, J., Henderson, R., Lashley, B., Zhang, X., Hassan, E.B., Perez, F., Mohan, D., Pittman, C.U., Mlsna, T., 2020. Biochar adsorbents with enhanced hydrophobicity for oil spill removal. ACS Appl. Mater. Interfaces 12, 9248–9260.
- Newcombe, G., Hayes, R., Drikas, M., 1993. Granular activated carbon: importance of surface properties in the adsorption of naturally occurring organics. Colloids Surf. A Physicochem. Eng. Asp. 78, 65–71.
- Oh, H., Yu, M., Takizawa, S., Ohgaki, S., 2006. Evaluation of PAC behavior and fouling formation in an integrated PAC–UF membrane for surface water treatment. Desalination 192, 54–62.
- Ojeda, G., Mattana, S., Àvila, A., Alcañiz, J.M., Volkmann, M., Bachmann, J., 2015. Are soil–water functions affected by biochar application? Geoderma 249–250, 1–11. Olsen, G.W., Mair, D.C., Lange, C.C., Harrington, L.M., Church, T.R., Goldberg, C.L.,
- Olsen, G.W., Mair, D.C., Lange, C.C., Harrington, L.M., Church, T.R., Goldberg, C.L., Herron, R.M., Hanna, H., Nobiletti, J.B., Rios, J.A., Reagen, W.K., Ley, C.A., 2017. Per- and polyfluoroalkyl substances (PFAS) in American Red Cross adult blood donors, 2000–2015. Environ. Res. 157, 87–95.

- Özcan, Y., Makineci, E., Özdemir, E., 2020. Biomass, carbon and nitrogen in single tree components of grey poplar (Populus × canescens) in an uncultivated habitat in Van, Turkey. Environ. Monit. Assess. 192.
- Regmi, P., Garcia Moscoso, J.L., Kumar, S., Cao, X., Mao, J., Schafran, G., 2012. Removal of copper and cadmium from aqueous solution using switchgrass biochar produced via hydrothermal carbonization process. J. Environ. Manag. 109, 61–69.
- Rong, X., Xie, M., Kong, L., Natarajan, V., Ma, L., Zhan, J., 2019. The magnetic biochar derived from banana peels as a persulfate activator for organic contaminants degradation. Chem. Eng. J. 372, 294–303.
- Sagbo, O., Sun, Y., Hao, A., Gu, P., 2008. Effect of PAC addition on MBR process for drinking water treatment. Separ. Purif. Technol. 58, 320–327.
- Shaaban, A., Se, S.-M., Dimin, M.F., Juoi, J.M., Husin, M.H., Mitan, N.M.M., 2014. Influence of heating temperature and holding time on biochars derived from rubber wood sawdust via slow pyrolysis. J. Anal. Appl. Pyrol. 107, 31–39.
- Sörengård, M., Östblom, E., Köhler, S., Ahrens, L., 2020. Adsorption behavior of per- and polyfluoralkyl substances (PFASs) to 44 inorganic and organic sorbents and use of dyes as proxies for PFAS sorption. J. Environ. Chem. Eng. 8, 103744.
- Suffet, I.H., 1980. An evaluation of activated carbon for drinking water treatment: a national academy of science report. J. AWWA (Am. Water Works Assoc.) 72, 41–50.
- Tarka, P., 2018. An overview of structural equation modeling: its beginnings, historical development, usefulness and controversies in the social sciences. Qual. Quantity 52, 313–354.
- Team, R.C., 2022. R: A Language and Environment for Statistical Computing. R Foundation for Statistical Computing, Vienna, Austria.
- Thompson, K.A., Shimabuku, K.K., Kearns, J.P., Knappe, D.R.U., Summers, R.S., Cook, S. M., 2016. Environmental comparison of biochar and activated carbon for tertiary wastewater treatment. Environ. Sci. Technol. 50, 11253–11262.
- Tomczyk, A., Sokołowska, Z., Boguta, P., 2020. Biochar physicochemical properties: pyrolysis temperature and feedstock kind effects. Rev. Environ. Sci. Biotechnol. 19, 101, 215
- USEPA, 2016. FACT SHEET PFOA & PFOS Drinking Water HealthAdvisories. U.S. Environmental Protection Agency (EPA). https://www.epa.gov/sites/default/files/2016-06/documents/drinkingwaterhealthadvisories pfoa pfos updated 5.31.16.pdf.
- USEPA, 2022. Drinking Water Health Advisories for PFOA and PFOS. U.S. Environmental Protection Agency (EPA). https://www.epa.gov/sdwa/drinking-water-health-advisories-pfoa-and-pfos.
- USEPA, 2023. Per- and Polyfluoroalkyl Substances (PFAS) Proposed PFAS National Primary Drinking Water Regulation. U.S. Environmental Protection Agency (EPA). https://www.epa.gov/sdwa/and-polyfluoroalkyl-substances-pfas.
- Valdés, H., Sánchez-Polo, M., Rivera-Utrilla, J., Zaror, C.A., 2002. Effect of ozone treatment on surface properties of activated carbon. Langmuir 18, 2111–2116.
- Wang, P., Peng, H., Adhikari, S., Higgins, B., Roy, P., Dai, W., Shi, X., 2020. Enhancement of biogas production from wastewater sludge via anaerobic digestion assisted with biochar amendment. Bioresour. Technol. 309, 123368.
- Wiersma, W., van der Ploeg, M.J., Sauren, I.J.M.H., Stoof, C.R., 2020. No effect of pyrolysis temperature and feedstock type on hydraulic properties of biochar and amended sandy soil. Geoderma 364, 114209.
- Xing, W., Ngo, H.H., Kim, S.H., Guo, W.S., Hagare, P., 2008. Adsorption and bioadsorption of granular activated carbon (GAC) for dissolved organic carbon (DOC) removal in wastewater. Bioresour. Technol. 99, 8674–8678.
- Yuan, J.-H., Xu, R.-K., Zhang, H., 2011. The forms of alkalis in the biochar produced from crop residues at different temperatures. Bioresour. Technol. 102, 3488–3497.
- Zhang, D., He, Q., Wang, M., Zhang, W., Liang, Y., 2021. Sorption of perfluoroalkylated substances (PFASs) onto granular activated carbon and biochar. Environ. Technol. 42, 1798–1809.
- Zhang, K., Sun, P., Faye, M.C.A.S., Zhang, Y., 2018. Characterization of biochar derived from rice husks and its potential in chlorobenzene degradation. Carbon 130, 730–740.